Front. Earth Sci. 2023, 17(2): 391–406
https://doi.org/10.1007/s11707-022-1005-2

RESEARCH ARTICLE

# Hybrid global gridded snow products and conceptual simulations of distributed snow budget: evaluation of different scenarios in a mountainous watershed

**Mercedeh TAHERI[1,2], Milad Shamsi ANBOOHI[1], Rahimeh MOUSAVI[3], Mohsen NASSERI (✉)[1]**

1 School of Civil Engineering, College of Engineering, University of Tehran, Tehran 1417935840, Iran
2 Department of Civil Engineering, University of Ottawa, Ottawa, Ontario K1N6N5, Canada
3 Department of Civil Engineering, Faculty of Engineering, University of Zanjan, Zanjan 45371-38791, Iran



**Abstract** Considering snowmelt in mountainous areas as the important source of streamflow, the snow accumulation/melting processes are vital for accurate simulation of the hydrological regimes. The lack of snow-related data and its uncertainties/conceptual ambiguity in snowpack modeling are the different challenges of developing hydro-climatological models. To tackle these challenges, Global Gridded Snow Products (GGSPs) are introduced, which effectively simplify the identification of the spatial characteristics of snow hydrological variables. This research aims to investigate the performance of multi-source GGSPs using multi-stage calibration strategies in hydrological modeling. The used GGSPs were Snow-Covered Area (SCA) and Snow Water Equivalent (SWE), implemented individually or jointly to calibrate an appropriate water balance model. The study area was a mountainous watershed located in Western Iran with a considerable contribution of snowmelt to the generated streamflow. The results showed that using GGSPs as complementary information in the calibration process, besides streamflow time series, could improve the modeling accuracy compared to the conventional calibration, which is only based on streamflow data. The SCA with NSE, KGE, and RMSE values varying within the ranges of 0.47–0.57, 0.54–0.65, and 4–6.88, respectively, outperformed the SWE with the corresponding metrics of 0.36–0.59, 0.47–0.60, and 5.22–7.46, respectively, in simulating the total streamflow of the watershed. In addition to the superiority of the SCA over SWE, the two-stage calibration strategy reduced the number of optimized parameters in each stage and the dependency of internal processes on the streamflow and improved the accuracy of the results compared with the conventional calibration strategy. On the other hand, the consistent contribution of snowmelt to the total generated streamflow (ranging from 0.9 to 1.47) and the ratio of snow melting to snowfall (ranging from 0.925 to 1.041) in different calibration strategies and models resulted in a reliable simulation of the model.

**Keywords** global gridded snow products, snow hydrology, multi-stage calibration strategy, hydro-climatological modeling, mountainous watershed

## 1 Introduction

Snowmelt plays a substantial role in generating streamflow over mountainous watersheds given the large amounts of snow storage in highlands, which are melted in warm seasons. This natural mechanism affects human-made development activities (such as agricultural production, water storage and supply, and ecosystem conservation) and hydro-climatological processes (such as drought and flash floods) (Immerzeel et al., 2009; Nemri and Kinnard, 2020). Therefore, simulating the snow mechanism is of high importance in achieving a realistic perspective of hydrological components in the water cycle of a mountainous watershed (Lévesque et al., 2008; Debele et al., 2010; Gao et al., 2020). However, there are some constraints, such as limited access to snowfall and snowmelt information, insufficient measurement networks, and relevant systematic errors intensified by steep slopes and turbulence flows (Taheri et al., 2022). These limitations lead to relatively substantial uncertainties about the modeling and make the verification of results challenging (Orsolini et al., 2019; Bian et al., 2019). To solve these issues, Global Gridded Snow Products (GGSPs) provide scientific communities

Received August 8, 2021; accepted May 25, 2022

E-mail: mnasseri@ut.ac.ir

with an unprecedented opportunity to achieve valuable spatiotemporal information (Parajka and Blöschl, 2008). The accuracy and accessibility of the products are not dependent on land surface characteristics (Parajka and Blöschl, 2008) and can dramatically reduce modeling barriers in mountainous areas.

The conventional calibration method based on recorded streamflow time series does not necessarily delineate the correct behavior of hydrological models and their internal processes (Refsgaard, 1997; Ajami et al., 2004; Reed et al., 2004; Khakbaz et al., 2012; Smith et al., 2012). This issue would become more critical when the recorded hydrometric information has unfilled gaps during the calibration period (Beven, 2011). In this regard, the use of GGSPs as calibration references can accurately define relationships between internal and external hydrological variables and, thus, lead to higher stability in the calibration process compared to the conventional method (Güntner et al., 1999; Seibert, 2000; Franz and Karsten, 2013; Li et al., 2021).

Snow-Covered Area (SCA) and Snow Water Equivalent (SWE) are the most important characteristics of the snow process in hydrological models. Optical remote sensing SCA products can provide beneficial spatial patterns of snow coverage. On the contrary, SWE obtained from Passive Micro-Wave (PMW) using snow depth and density can represent a better temporal continuity due to the lack of illumination impact (clouds and nights) (Roy et al., 2010; Bigdeli et al., 2021). However, coarse spatial resolution is the major problem of SWE products (Derksen et al., 2005; Pulliainen, 2006; Dai et al., 2015), being the main reason behind their less use in the watershed-scale hydrological modeling compared to SCA (Dietz et al., 2012).

Remotely sensed SCA patterns can be considered as a suitable source of information for indirect constraining of the snow model parameters. Therefore, various approaches have been developed to highlight the application of these data in hydrological and land surface models as follows.

1) Direct use of SCA as the input variable of the conceptual snow model (Martinec et al., 1994; Tekeli et al., 2005; Li and Williams, 2008).

2) Indirect use of SCA in assimilation and correction procedures (Rodell and Houser, 2004; Andreadis and Lettenmaier, 2006; Clark et al., 2006; Slater and Clark, 2006; Zaitchik and Rodell, 2009; Roy et al., 2010; Yatheendradas et al., 2012; Thirel et al., 2013).

3) Indirect use of SCA as a reference to calibrate, validate, and evaluate hydrological models (Cline et al., 1998; Engeset et al., 2003; Zappa et al., 2003; Dressler et al., 2006; Udnæs et al., 2007; Parajka and Blöschl., 2008; Corbari et al., 2009; Şorman et al., 2009; Finger et al., 2011; Franz and Karsten., 2013; Duethmann et al., 2014; He et al., 2014; Shrestha et al., 2014; Shrestha et al., 2015; Chen et al., 2017; Han et al., 2019; Riboust et al., 2019; Nemri and Kinnard., 2020; Li et al., 2021).

In the last approach, the SCA and the streamflow time series were used to calibrate the hydrological model via single- or multi-objective optimization methods. The leading researchers in this area are Parajka and Blöschl (2008), who simultaneously used MODIS snow cover product and streamflow values to calibrate the semi-distributed HBV (Hydrologiska Byrans Vattenbalans-avdelning) model in 148 watersheds in Austria using the original Terra and Aqua MODIS images. Most of the studies in this field have concluded that the application of snow cover has improved the performance of hydrological simulations (e.g., Han et al., 2019; Chen et al., 2017).

The mentioned studies have evaluated snowpack models using only one snow-related product (i.e., SCA), while using multiple information may effectively improve the simulation/recognition of snow hydrology and streamflow. In addition, the consistency of the calibrated hydrological models with different combinations of data sets indicates successful modeling with reliable accuracy. Hence, this research is aimed at using multi-source GGSPs (i.e., SCA and SWE) beside recorded streamflow time series as calibration references to look for a reliable framework for snow hydrology and streamflow simulation. More clearly, the novelty of the research is the use of SWE data combined with the SCA product and streamflow values through multi-stage calibration procedures separately and in a combined way to simulate the snowmelt and streamflow of the watershed of interest. It is worth noting that the use of SWE in the calibration process of the snow budget model provides a straightforward mechanism to achieve optimal parameters.

Among different water balance concepts, a suitable monthly water balance model was calibrated for the period of 2000 to 2015 to accomplish the purpose of the study in a mountainous watershed located in western Iran. The MODIS SCA and ERA5-Land SWE were the desired snow products used in the current research. In addition, Guo et al (2005) and McCabe and Markstrom (2007) snow modules were employed to quantify the interaction between snow and other modules of the water balance model. The following sections describe the ground and global gridded snow data, modeling procedure, and the results, respectively.

## 2 Study area and data

### 2.1 Study area

Gheshlagh is a mountainous watershed located the upstream of Gheshlagh Dam between the geographical coordinates of 46°20′E to 47°46′E longitude and 35°24′N to 35°43′N latitude (Fig. 1). The watershed's altitude varies from 1470 m to 2874 m with an average of 1960.4 m,

and it is classified as one of the mountainous and highland watersheds in Iran. The watershed area is about 1062.12 km$^2$, with an average slope of 16.74%. In addition, its average annual rainfall and temperature are 454.4 mm and 13.3°C, respectively.

### 2.2 Data

The local and ground-based data sets used in the current research included precipitation, air temperature, pan evaporation, and recorded streamflow at the watershed outlet. The average monthly precipitation was estimated using the optimized Moving Least Square (MLS) method (Taheri et al., 2020; Amini and Nasseri, 2021) on a regular grid domain over the watershed (5 × 5 km$^2$). In addition, the air temperature and pan evaporation values, which belong to the climatological network of the Iran Ministry of Power and the National Meteorological Organization, were obtained from the linear-gradient method over the computational grids.

The GGSPs used in the current study included the MODIS SCA (MOD10CM) and the ERA5-Land SWE with spatial resolutions of 5 km and 10 km, respectively. The MOD10CM product is yielded by averaging daily snow cover observations of MOD10C1 (Hall and Riggs, 2015). Moreover, the ERA5-Land SWE was estimated based on the H-TESSEL (the Tiled ECMWF Scheme for Surface Exchanges over land incorporating land surface hydrology) and data assimilation techniques (Muñoz-Sabater, 2019). The monthly time scale was adopted for the used snow products to be compatible with the selected water balance model and reduce cloud cover effects. Given the high absolute accuracy of the MODIS SCA product (about 93%) (Hall and Riggs, 2007), it is known as appropriate supporting information for the modeling of snow hydrology. On the other hand, SWE, an informative variable in snow hydrology, is defined as the actual amount of water stored in the snowpack. Although the SWE product has received less attention in hydrological modeling due to the uncertainty forced by its coarse resolution (Yang et al., 2020; Kim et al., 2021), the ERA5-Land SWE with a relatively suitable spatial resolution may be an acceptable option for watershed-scale modeling.

## 3 Modeling procedure

To investigate the hydro-climatological behavior of the study area, several conceptual monthly water balance models compatible with its geological, physiographical, and hydrological conditions were considered to find the most suitable model. Given the mountainous climate and considerable snow coverage of the watershed, the selected water balance model had to have snow hydrology features (i.e., snow accumulation and melting). Therefore, the performance of several conceptual snow models was evaluated for structural modification of the selected water balance model. On the other hand, three scenarios were planned to explore different calibration processes in determining the snow hydrology and watershed streamflow through global-scale products. Figure 2 depicts the applied conceptual water balance flowchart.

### 3.1 Monthly water balance model

As previously mentioned, the water balance model had to be capable of modeling the process of snow accumulation and snow melting, given the mountainous nature of the study area. Therefore, the following monthly water balance models were evaluated: *abc* (Vogel and Sankarasubramanian, 2003) that is modified by snow budget, the water balance models developed by Rao and Al-Wagdany (1995), Guo et al. (2005) (that is modified by snow budget), Jazim (2006) (that is modified by snow budget), Karpouzos et al. (2011), and Wang et al. (2013),

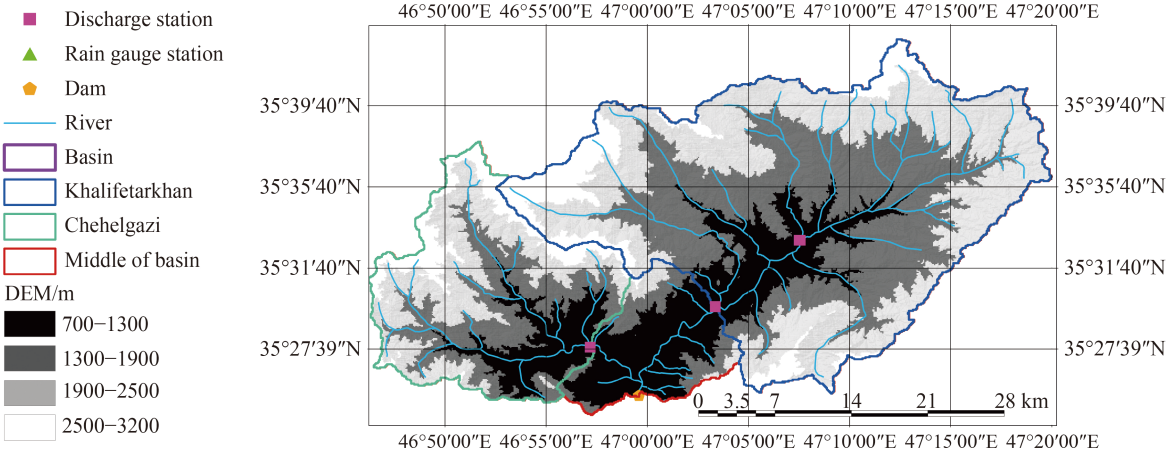


**Fig. 1** Gheshlagh watershed along with hydrometric stations, rain gauges, river network, and altitude image.

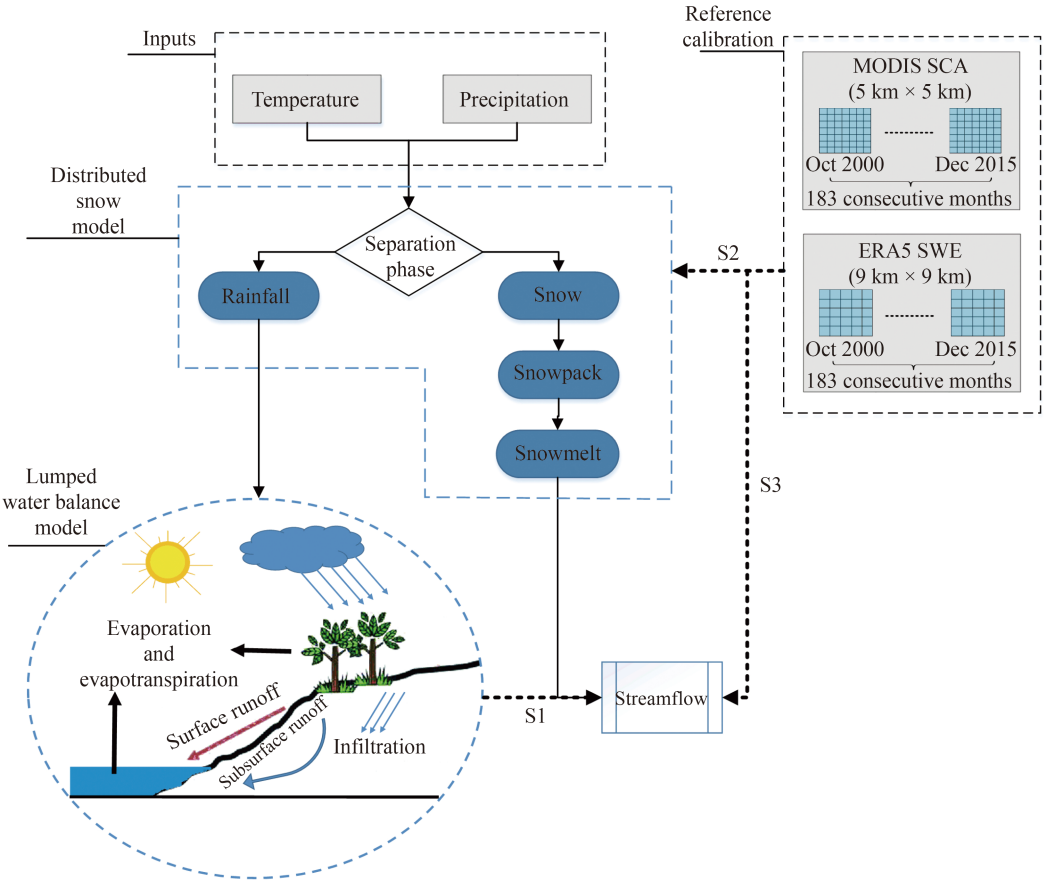


**Fig. 2** The proposed framework to simulate the snowmelt and total runoff using one and two-stage calibration strategies and GGSPs

and WASMOD-M (Widén-Nilsson et al., 2007). The best model, selected based on different statistics, is reported in Section 4.1.

### 3.2 Snowpack model

Since precipitation is in the form of snow, rain, and their combination in mountainous areas, the accurate separation of rainfall and snow affects the precision of streamflow simulation. Moreover, the melting process and its parameters determine the amount of snowmelt that participates in generating the watershed streamflow. Therefore, given the importance of the snowpack simulation, several conceptual models of snow hydrology, including models developed by Xu (1999), Guo et al. (2005), McCabe and Markstrom (2007), Parajka et al. (2007), and Widén-Nilsson et al. (2007) (WASMOD-M) were used to modify the water balance model. The mentioned models utilize the degree-day temperature index by separating precipitation into snow and rain based on temperature thresholds and melting rate.

### 3.3 Modeling scenarios

In most cases, hydrological models are calibrated using streamflow time series recorded at hydrometric outlet stations (Rabuffetti et al., 2008). Although this type of calibration is suitable for tuning the model output as an external response, it is not necessarily appropriate for detecting the internal hydrological connections of the water cycle. In addition, the dependency of internal processes such as the snow module on the outlet's streamflow might be greater in the conventional calibration procedure. Therefore, a two-stage calibration method was used, as well as multi-source information, to reduce the dependency of the snow process on the streamflow and constrain the hydrological model. In this regard, SCA and SWE products were considered new references to calibrate the water balance model under the proposed scenarios. These scenarios, categorized into three major groups, are explained in the following.

1) **Scenario 1 (S1).** The calibration process was completed based on streamflow time series to optimize all the model parameters in one stage. This scenario, which is a conventional approach to calibrate hydrological models in most studies, is called the benchmark scenario herein.

2) **Scenario 2 (S2).** In the first stage, the parameters related to the snow module were calculated independently from the water balance model. Accordingly, three data

sets (SCA, SWE, and their combination) were used separately as the calibration references to find the optimal parameters of the conceptual snow model. In the second stage, the optimized parameter set, along with other input variables, was applied to the water balance model to calibrate the remaining parameters by adjusting the simulated and recorded streamflow time series.

3) **Scenario 3 (S3).** All parameters of the modules (snowpack and water balance) were calibrated simultaneously. In this scenario, the combined data of SCA & streamflow, SWE & streamflow, and SCA & SWE & streamflow were used to calibrate the hydrological model.

### 3.4 Calibration methods

Normal Mean Square Error (NMSE) is the first objective function used in an optimization process when streamflow is the only reference to calibrate (Eq. (1)). Suppose SCA and SWE products are utilized as the calibration targets. In that case, the Sum Absolute Error (SAE) and the Distance term of Kling–Gupta Efficiency (DKGE) metrics (Knoben et al., 2019) are employed as the objective functions, respectively (Eqs. (2) and (3)).

$$\mathrm{Obj}_1 = \frac{1}{n}\frac{\sum_{i=1}^{n}\left(Q_i^{\mathrm{obs}} - Q_i^{\mathrm{sim}}\right)^2}{Var_{\mathrm{obs}}}, \tag{1}$$

$$\mathrm{Obj}_2 = \sum_{i=1}^{n} abs\left(SCA_i^{\mathrm{obs}} - SCA_i^{\mathrm{sim}}\right), \tag{2}$$

$$\mathrm{Obj}_3 = \left(R_{\mathrm{obs\_SWE}}^{\mathrm{sim\_SWE}} - 1\right)^2 + \left(\frac{\sigma_{\mathrm{sim}}^{\mathrm{SWE}}}{\sigma_{\mathrm{obs}}^{\mathrm{SWE}}} - 1\right)^2 + \left(\frac{\overline{\mathrm{SWE}_{\mathrm{sim}}}}{\overline{\mathrm{SWE}_{\mathrm{obs}}}} - 1\right)^2. \tag{3}$$

In Eq. (1), $n$ is the number of data, $Q_i^{\mathrm{obs}}$ and $Q_i^{\mathrm{sim}}$ are observed and simulated streamflows, respectively, and $Var_{\mathrm{Obs}}$ is the variance of the observed streamflow values. In Eq. (2), $SCA_i^{\mathrm{obs}}$ is the observed snow cover area, and $SCA_i^{\mathrm{sim}}$ indicates simulated snow cover area, which is calculated based on the snowpack depth by defining a threshold so that if the simulated snowpack depth is greater or shallower than it, $SCA_i^{\mathrm{sim}}$ would be equal to one or zero, respectively. In Eq. (3), $R_{\mathrm{obs\_SWE}}^{\mathrm{sim\_SWE}}$ is the Correlation Coefficient (CC or $R$) between observed and simulated SWEs, $\sigma_{\mathrm{sim}}^{\mathrm{SWE}}$ and $\sigma_{\mathrm{obs}}^{\mathrm{SWE}}$ are the standard deviation of the simulated and observed SWEs, respectively, and $\overline{\mathrm{SWE}_{\mathrm{sim}}}$ and $\overline{\mathrm{SWE}_{\mathrm{obs}}}$ indicate the averages of the simulated and observed SWE values over the computational period, respectively. It should be mentioned that $\mathrm{SWE}_{\mathrm{sim}}$ is estimated based on the simulated snowpack depth multiplied by snow density, which is a parameter acquired through the calibration process.

A weighted linear combination of the above statistical metrics was used in the proposed combined scenarios to define the fitness functions. Hence, the objective function for the SCA & streamflow combination was the weighted average of NMSE and SAE (Eq. (4)). The weighted average of NMSE and DKGE between streamflow and SWE values was the objective function for the SWE & streamflow combination (Eq. (5)). In addition, the objective function used to calibrate the streamflow combined with SCA and SWE is presented in Eq. (6), and the one used for the combination of SCA and SWE is shown in Eq. (7).

$$\mathrm{Obj}_4 = \mathrm{NMSE}_{\mathrm{Streamflow}} + 0.01\mathrm{SAE}_{\mathrm{SCA}}, \tag{4}$$

$$\mathrm{Obj}_5 = \mathrm{NMSE}_{\mathrm{Streamflow}} + \mathrm{DKGE}_{\mathrm{SWE}}, \tag{5}$$

$$\mathrm{Obj}_6 = \mathrm{NMSE}_{\mathrm{Streamflow}} + 0.01\mathrm{SAE}_{\mathrm{SCA}} + \mathrm{DKGE}_{\mathrm{SWE}}, \tag{6}$$

$$\mathrm{Obj}_7 = 0.01\mathrm{SAE}_{\mathrm{SCA}} + \mathrm{DKGE}_{\mathrm{SWE}}. \tag{7}$$

It is worth noting that the comparison between the observed and simulated SWEs was performed directly in the calibration step using the SWE reference data while calibrating the model through SCA values needs the data set to be converted to binary values (zero and one) using two threshold parameters of snow cover ($T_1$, $T_2$). Table 1 depicts the parameter sets of different scenarios, references, calibration steps, and objective functions. According to the table, $T_{\mathrm{rain}}$, $T_{\mathrm{snow}}$, and $K_{\mathrm{sn}}$ are the three parameters related to the process of separating snow/rain and generating snowmelt. The SM parameter is defined to convert the simulated SCA to binary values. If the simulated SCA is equal to or greater than SM, its value is one; otherwise, it is zero. Snow cover thresholds ($T_1$ and $T_2$) are also used to convert SCA products to binary codes. In other words, the SCA values greater and equal to/lower than $T_1$ are assigned the highest and lowest binary values, respectively. The remaining parameters belong to the generation of surface ($K_g$) and subsurface ($K_s$) streamflows and maximum soil moisture storage ($S_{\max}$). The Shuffled Complex Evolution (SCE-UA) algorithm, first developed by Duan et al. (1992), was employed to calibrate the models' parameters. The evolution process is repeated until certain convergence criteria are satisfied. In this paper, three stopping criteria were used to terminate each optimization process. The first criterion was reaching 10000 function evaluations of the trial. By the second criterion, when sample parameter convergence occurred (the region would span by the sample converged down to within $10^{-6}$ of the parameter range in each direction), the algorithm terminated without reducing the best fitness value below $10^{-3}$. According to the last criterion, when the best fitness value remained constant for 30 successive iterations, the optimization procedure was stopped.

**Table 1** Parameter set of hydrological model by scenario, calibration stage and reference, and objective function

| Scenario | Calibration Stage | | Parameters | | | | | | | | | | Calibration Reference | Objective Function |
|---|---|---|---|---|---|---|---|---|---|---|---|---|---|---|
| | ו | וו | Sub-surface runoff coefficient ($K_g$) | Surface runoff coefficient ($K_s$) | Maximum soil moisture storage ($S_{max}$) | Rainfall threshold temperature ($T_{rain}$) | Snowfall threshold temperature ($T_{snow}$) | Snowmelt coefficient ($K_{sn}$) | Snow density (P) | SCA threshold to convert simulated SCA to 1 or 0 (SM) | SCA threshold to convert satellite SCA to 1 ($T_1$) | SCA threshold to convert satellite SCA to 0 ($T_2$) | | |
| **S1** | * | | * | * | * | * | * | * | | | | | Runoff | $Obj_1$ |
| **S2** | * | | | | | | | * | * | * | * | * | SCA | $Obj_2$ |
| | * | | | | | * | * | * | * | | | | SWE | $Obj_3$ |
| | * | | | | | | | * | | * | * | * | SCA and SWE | $Obj_7$ |
| | | * | * | * | * | | | | | | | | Runoff | $Obj_1$ |
| **S3** | * | | * | * | * | * | * | * | * | * | * | * | SCA and Runoff | $Obj_4$ |
| | * | | * | * | * | * | * | * | * | | | | SWE and Runoff | $Obj_5$ |
| | * | | * | * | * | * | * | * | * | * | * | * | SCA and SWE and Runoff | $Obj_6$ |

### 3.5 Evaluation statistics

The Root Mean Square Error (RMSE), as a dissimilarity metric, along with the Nash–Sutcliffe Efficiency (NSE) and $R^2$, as the most well-known similarity metrics, and KGE, as a hybrid statistical metric, were utilized to compare the observed and simulated streamflows under the proposed scenarios. The following equations show their mathematical formulations:

$$\mathrm{RMSE} = \sqrt{\frac{\sum_{i=1}^{n}(Q_i^{\mathrm{obs}} - Q_i^{\mathrm{sim}})^2}{N}}, \tag{8}$$

$$\mathrm{NSE} = 1 - \frac{\sum_{i=1}^{n}(Q_i^{\mathrm{obs}} - Q_i^{\mathrm{sim}})^2}{\sum_{i=1}^{n}(Q_i^{\mathrm{obs}} - \overline{Q_{\mathrm{obs}}})^2}, \tag{9}$$

$$R^2 = \frac{cov(Q_i^{\mathrm{obs}}, Q_i^{\mathrm{sim}})}{\sqrt{Var\left(Q_i^{\mathrm{obs}}\right) \times Var\left(Q_i^{\mathrm{sim}}\right)}}, \tag{10}$$

$$KGE = 1 - \sqrt{(R-1)^2 + \left(\frac{\sigma_{\mathrm{sim}}}{\sigma_{\mathrm{obs}}} - 1\right)^2 + \left(\frac{\overline{Q_{\mathrm{sim}}}}{\overline{Q_{\mathrm{obs}}}} - 1\right)^2}. \tag{11}$$

In addition to the metrics above, the Relative Error (RE) and Heidke Skill Score (HSS) (Roebber, 2009) were employed to evaluate the spatial distribution of the simulated SWE and SCA over the time period. The RE indicates the normalized sum residual between the observed and simulated target. The greater the difference between the simulated values and the observations, the worse the modeling performance. On the other hand, the HSS measures the simulation accuracy randomly, varying between −1 (the worst performance) and 1 (the best performance). The formulations of these indicators are as follows:

$$\mathrm{RE} = \frac{\sum_{i=1}^{n}(\mathrm{SWE}_i^{\mathrm{obs}} - \mathrm{SWE}_i^{\mathrm{sim}})}{\sum_{i=1}^{n}\left(\mathrm{SWE}_i^{\mathrm{obs}}\right)}, \tag{12}$$

$$\mathrm{HSS} = \frac{2 \times (H \times Z - M \times F)}{(H+M)(M+Z) + (H+F)(F+Z)}. \tag{13}$$

In Eq. (13), $H$, $F$, $M$, and $Z$ are the numbers of correct estimates, incorrect estimates, lost estimates, and correct negative estimates, respectively.

## 4 Results and discussion

### 4.1 Statistical performance of the water balance and snow models

Table 2 shows the statistical metrics, including NSE and R, for snowpack and water balance models. As can be seen, the conceptual model developed by Wang et al. (2013) generally has higher NSE and R values than other water balance models. Therefore, it was adopted as the best water balance model. Furthermore, the Modified Wang Water Balance (MWWB) model with Guo and McCabe's snowpack modules (named MWWB-1 and MWWB-2, respectively) has the best performance.

### 4.2 Assessment of the scenarios

In this section, the statistical performance of the water balance models (MWWB-1 and MWWB-2) is evaluated using the NSE, KGE, and RMSE metrics under different calibration scenarios, as depicted in Fig. 3. The NSE, KGE, and RMSE values equaled (0.42, 0.43), (0.59, 0.468), and (3.02, 7.14) for the MWWB1 and MWWB2, respectively, under the first scenario. Meanwhile, the corresponding metrics varied within the ranges of 0.236–0.597, 0.494–0.65, and 4.0–8.27 for the MWWB1 and 0.50–0.52, 0.54–0.56, and 5.06–5.3 for the MWWB2, respectively, when the second scenario was used with different reference combinations. Moreover, their ranges equaled 0.16–0.47, 0.46–0.61, and 6.88–8.3 for the MWWB1 and 0.21–0.54, 0.4–0.6, and 4.2–6.3, respectively, when the third scenario was utilized with different data combinations. Accordingly, the second and third scenarios generally outperformed the first one (the benchmark scenario). Moreover, the first scenario had the highest RMSE for the MWWB-2 (i.e., 7.14) and the lowest RMSE for the MWWB-1 (i.e., 3.02). Therefore, it can be inferred that the use of auxiliary information combined with streamflow values can improve the calibration performance of the hydrological model, increasing the accuracy of the simulated streamflow.

The second scenario had a smaller error and a higher similarity index than the third. This means a two-stage calibration process, which is implemented to reduce the number of parameters for each optimization step and the dependency of internal hydrological processes on the streamflow, is capable of improving the accuracy of simulations. It is necessary to notice that the optimization time for a complex model with a large number of parameters can be reduced by implementing the multi-stage calibration strategy.

On the other hand, the NSE, KGE, and RMSE varied within the ranges of 0.47–0.57, 0.54–0.65, and 4–6.88 under the second and third scenarios using the SCA & streamflow calibration reference, 0.36–0.59, 0.47–0.6, and 5.22–7.46 using the SWE & streamflow calibration reference, and 0.16–0.5, 0.39–0.56, and 5.3–8.29 using the SCA & SWE & streamflow as the calibration reference, respectively. Therefore, the hydrological model performances were better when using SCA & streamflow and SWE & streamflow combinations separately than using their combined mode (i.e., SCA & SWE & streamflow). Furthermore, SCA observations

outperformed the SWE in estimating the watershed streamflow, which can be attributed to the following reasons. Unlike other data, ERA5-land SWE data suffer from ignoring snow depth measurements that are mainly assimilated into the reanalysis data. Moreover, lack of blown snow sublimation in the calculation process of snow water equivalent and snowfall misestimation were other vague factors affecting the SWE results. The resolution of the reanalysis data that leads to a smoothed orography can also affect the retrieval accuracy of SWE, especially in highlands. In addition to internal uncertainties caused by the computational method, the mismatch of spatial scales that occurred between the SWE data (10 km) and the model (5 km) is another possible reason, while in the case of SCA products, the spatial resolutions of SAC and model were the same (5 km). It is worth noting that SCA products obtained from MODIS also had some uncertainties in providing

**Table 2** NSE and CC indicators for monthly water balance conceptual models and snowpack simulation modules

| | | NSE | | *R* | |
|---|---|---|---|---|---|
| | | Calibration | Validation | Calibration | Validation |
| **Water balance model** | Wang | 0.72 | 0.42 | 0.73 | 0.68 |
| | abc | 0.37 | 0.53 | 0.59 | 0.60 |
| | WASMOD-M | 0.34 | 0.55 | 0.59 | 0.56 |
| | RAO | −0.11 | 0.30 | 0.31 | 0.24 |
| | Karpouzos | 0.04 | 0.40 | 0.31 | 0.40 |
| | Guo | 0.18 | 0.50 | 0.64 | 0.64 |
| | Jazim | 0.31 | 0.42 | 0.55 | 0.65 |
| **Water balance model combined with snowpack module** | Wang-Guo | 0.73 | 0.42 | 0.74 | 0.68 |
| | Wang- McCabe | 0.671 | 0.434 | 0.825 | 0.66 |
| | Wang-Xu | 0.012 | −0.099 | 0.497 | 0.383 |
| | Wang-Parajaka | −0.117 | −0.104 | – | – |
| | Wang-WASMOD-M | −0.128 | −0.118 | – | – |

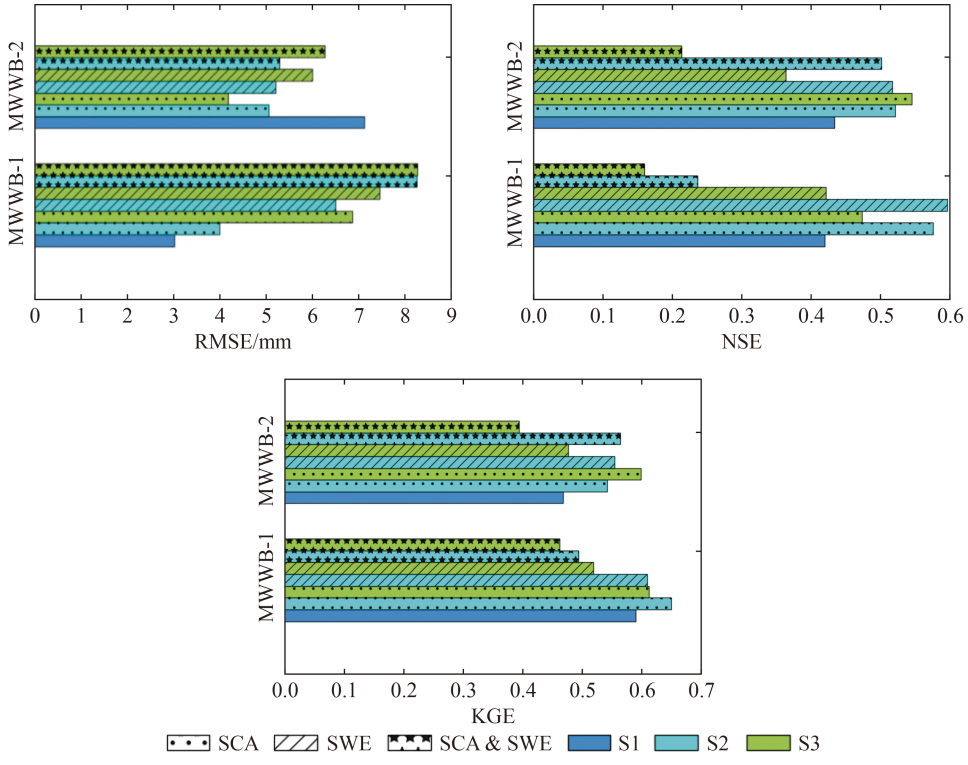


**Fig. 3** NSE, KGE, and RMSE (mm) metrics for the proposed scenarios using SCA, SWE, and SCA&SWE products and hydrologic models (MWWB-1 and MWWB-2).

spatiotemporal patterns of SCA. The most important factor affecting snow detection is imprecise cloud/snow discrimination by optical sensors (Hall and Riggs, 2007). This issue occurs in cloud-shadowed areas or areas with thin, sparse snow coverage due to the misidentification between snow and cloud. However, in the current paper, the monthly time scale for retrieving SCA products was adopted to employ the days with the clearest surface views and minimize the errors. That is why the SCA products outperformed the SWE products. Besides the mentioned factors, considering the snow density as a parameter calibrated by the model, which is constant for the watershed, can reduce the accuracy of SWE results followed by simulated streamflow.

### 4.3 Simulation of streamflow

**Calibration with the SCA product.** Figure 4(a) depicts the time series of the simulated streamflow at the watershed outlet (from 2000 to 2015) achieved by SCA observations as the calibration reference for different scenarios and models. The lowest and highest $R^2$ values belonged to the first and third scenarios and the MWWB-1 and MWWB-2 hydrological models, respectively. In addition, all scenarios captured the temporal variations of streamflow well. However, the first scenario of both models performed poorly in simulating peak values of the monthly streamflow.

**Calibration with the SWE product.** Figure 4(b) demonstrates the time series of the simulated streamflow during the computational period of 2000 to 2015 accomplished from SWE data as the calibration reference for different scenarios and models. Similar to the previous case, the lowest and highest $R^2$ belonged to the first and third scenarios of the MWWB-1 and MWWB-2 models, respectively. Furthermore, the second and third scenarios outperformed the first scenario, particularly in detecting the high streamflow values. However, the streamflow peaks (and valleys) simulated by all scenarios were generally well-captured in comparison with the target values.

**Calibration with SCA and SWE products.** Figure 4(c) presents the simulated streamflow time series from 2000 to 2015 that are achieved using SCA and SWE products as the calibration references for the proposed scenarios and models. According to the figure, the lowest and highest $R^2$ belonged to the third and second scenarios of the MWWB-1 and MWWB-2 models, respectively. In addition, S2 and S3 performed worse and better than S1 (benchmark scenario) for MWWB-1 and MWWB-2 models, respectively. Since the second and third scenarios underestimated the peak streamflow values, the combination of SCA and SWE products would not be suitable as calibration references compared with using each product separately for the studied watershed.

As can be concluded, the second and third scenarios outperformed the benchmark scenario (the first scenario) from the statistical point of view ($R^2$), with the performance of the second scenario being slightly better than the third one. On the other hand, the statistical metrics of the calibrated water balance models were more appropriate when using SCA and SWE individually. It is worth noting that using SCA and SWE separately did not show a significant superiority over each other in terms of $R^2$ in the calibration process.

### 4.4 Spatial distribution of HSS and RE

Figure 5 demonstrates the spatial distribution of the HSS for the monthly average values of SCA over the computational period. The maximum HSS value was 0.86 when the SCA & SWE combination was used to calibrate the model, and it equaled 0.95 when the model was calibrated using the SCA product by itself. In most cases, the central and southern areas of the watershed, located in low-altitude parts, had the lowest HSS values, while the northern parts, especially near the highlands, had the highest HSS values. The results indicated the appropriate compatibility of the simulated SCA with the SCA observations in the highlands and snow-covered areas, whereas the differences between the simulated and observed SCA were considerable in plains with the lowest elevation (mainly without snow). This can be due to a recurring fusion between cloud and snow caused by combining daily snow errors during a month (Hall and Riggs, 2021). It is worth noting that the spatial patterns of the HSS were almost the same under both calibration scenarios.

Figure 6 depicts the spatial pattern of the RE metric for SWE throughout the computational period. According to the figure, the mountainous areas of the watershed, especially the north-eastern and south-eastern parts, had the highest positive RE values. Therefore, due to the orography smoothing caused by the resolution of reanalysis, the model overestimated the SWE values in the highlands. On the other hand, the central and south-western parts of the watershed mostly had negative RE values meaning underestimated values of the simulated SWE compared to the observed values over low-altitude areas. The simulation error of the conceptual model was minimal (close to zero) in the middle altitudinal parts of the watershed, located between the highlands and the low-altitude flat areas. The maximum values of RE in calibration by SWE and SCA & SWE equaled 0.8 and 0.9, respectively. The RE index followed a spatial pattern similar to that of the HSS metric in all scenarios and models.

In summary, the individual use of SCA and SWE products in calibrating the models to estimate snow cover and snow water equivalent revealed a better statistical performance than their combined use. Given the better values of HSS than the RE values, it can be concluded that the hydrological models had better performance in

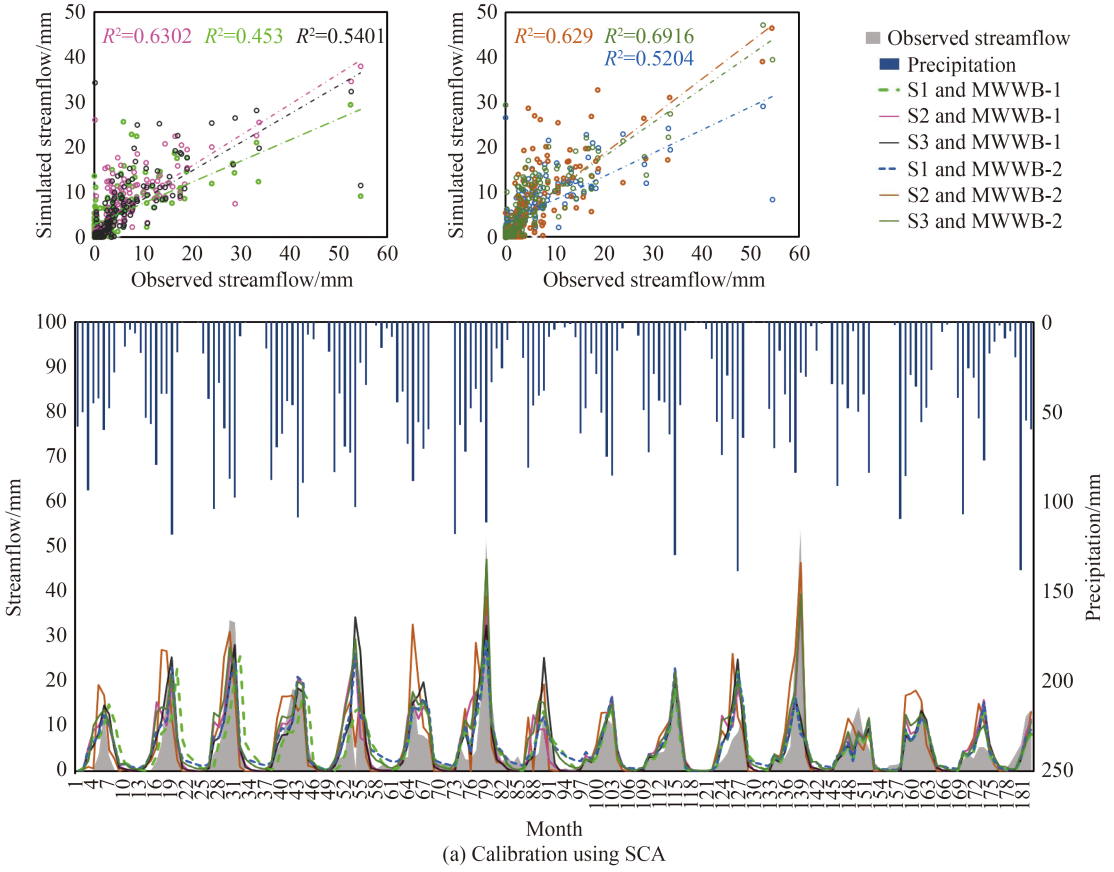


(a) Calibration using SCA

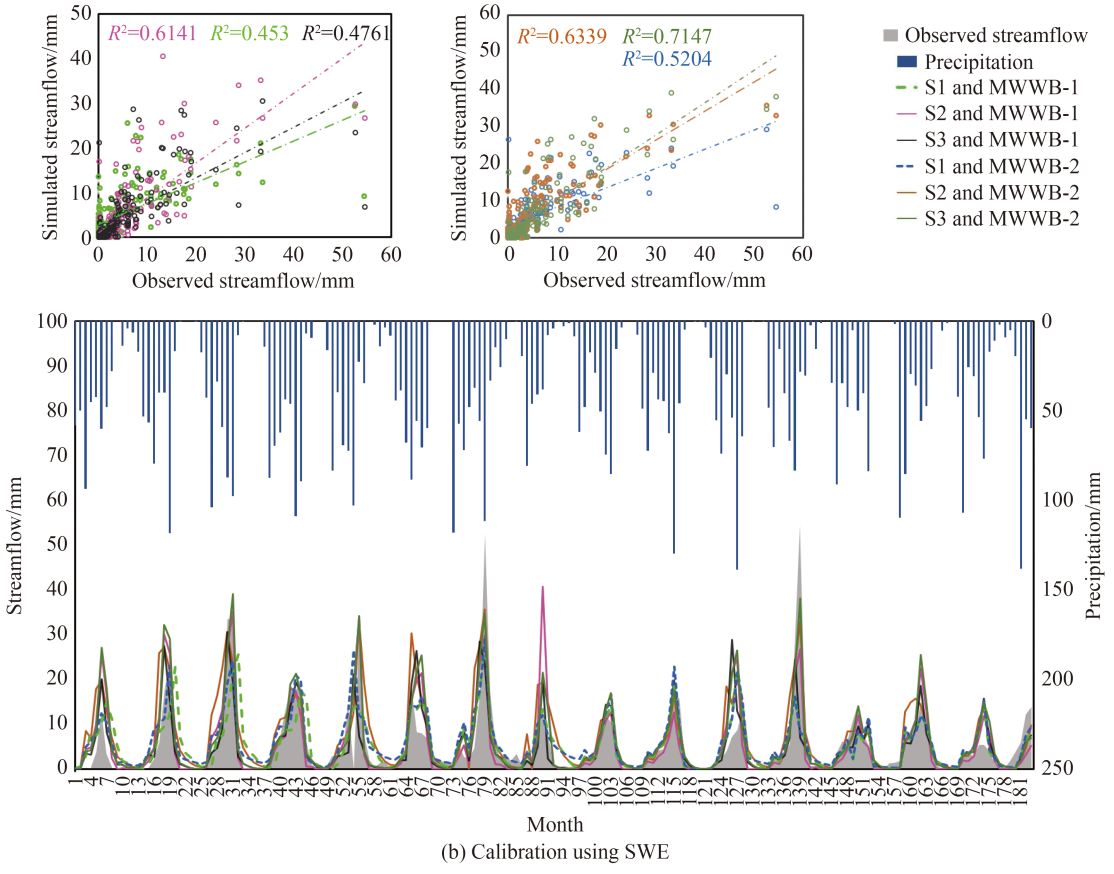


(b) Calibration using SWE

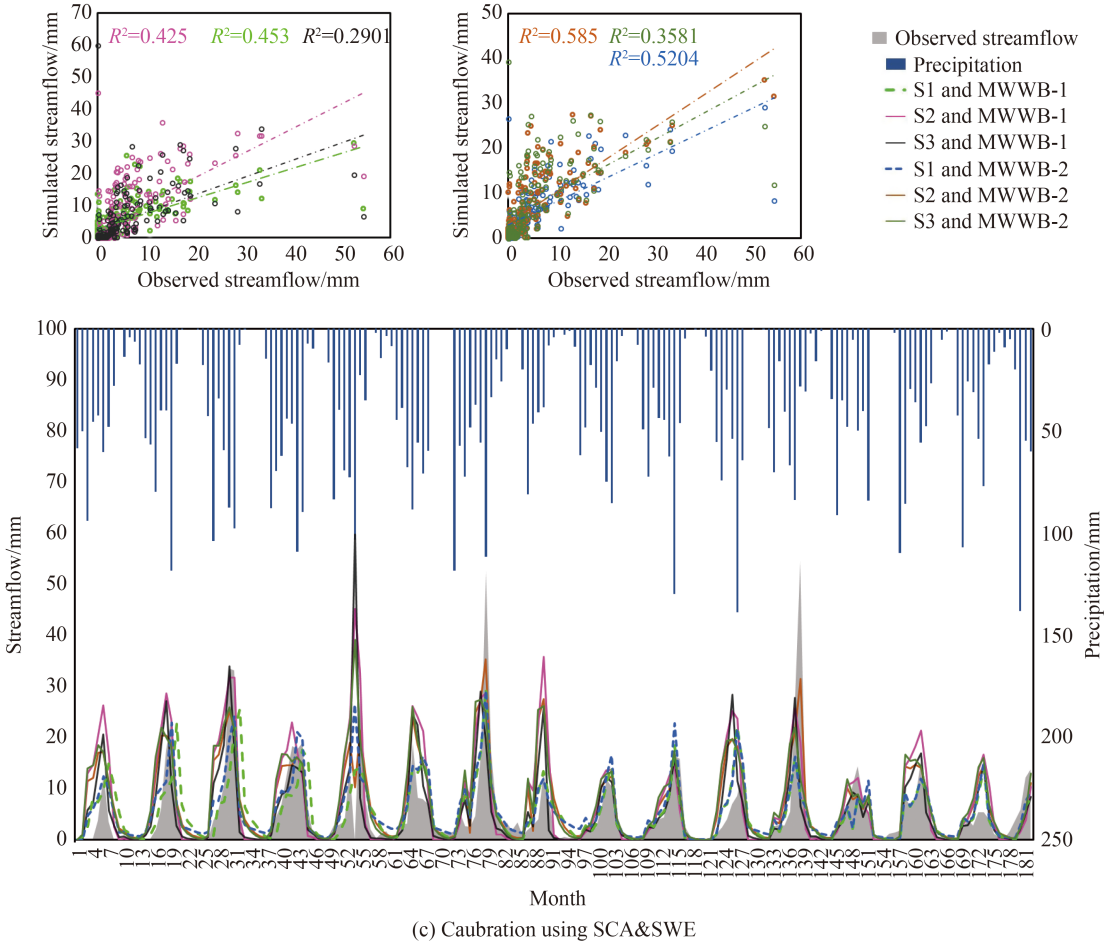


**Fig. 4** Time series of the observed and simulated streamflow during the period of 2000–2015 based on the proposed calibration scenarios and hydrologic models, (a) calibration using SCA, (b) calibration using SWE, (c) calibration using SCA & SWE.

estimating snow cover than snow water equivalent. This can be attributed to some factors like inherent uncertainty in the calculation process of the SWE product, spatial scale mismatch between the SWE data (10 km) and the model (5 km), the smoothed orography caused by reanalysis resolution, and the assumption of constant snow density for the watershed (as a parameter achieved by calibration).

### 4.5 Contribution of snow in the watershed hydrology

Table 3 presents the contribution of meltwater to the total generated streamflow under different scenarios from 2000 to 2015. Accordingly, the contribution of snowmelt to the generated streamflow for both models (MWWB1 and MWWB2) varied within the ranges of 75%–76%, 73%–74%, and 72%–80% under the second scenario (S2) using the SCA, SWE, and SCA & SWE data, respectively. Meanwhile, its ranges equaled 61%–71%, 60%–68%, and 62%–71% under the third scenario (S3) using the SCA, SWE, and SCA & SWE data, respectively.

The high values of the snowmelt contribution indicated that the melting process played a significant role in generating streamflow in the watershed. Based on the results, the difference in ratios caused by calibrating the models using various scenarios and references (SCA, SWE, and SCA & SWE) were insignificant. The greatest differences were 8% and 10% belonging to S2 and S3 scenarios, respectively, which could be due to the different structures of the snowpack modules. In addition to the individual data sets, the ratio of the snowmelt to the streamflow was calculated for each pair of data sets (i.e., SCA/SWE, SWE/SCA & SWE, and SCA/SCA & SWE). This way, the SCA/SWE (the contribution of snowmelt in generating streamflow when the models were calibrated by SCA versus the calibrated model using SWE), SWE/SCA & SWE (the contribution of snowmelt in generating streamflow when the models were calibrated by SWE versus the calibrated model via SCA & SWE), and SCA/SCA & SWE (the contribution of snowmelt in generating streamflow when the models were calibrated by SCA versus the calibrated model using SCA & SWE) in S2 varied between 1.01 and 1.04, 0.9–1.03, and 0.94–1.04, respectively. Moreover, these ratios for S3 varied between 1.04 and 1.045, 0.94–0.96, and 0.98–1, correspondingly.

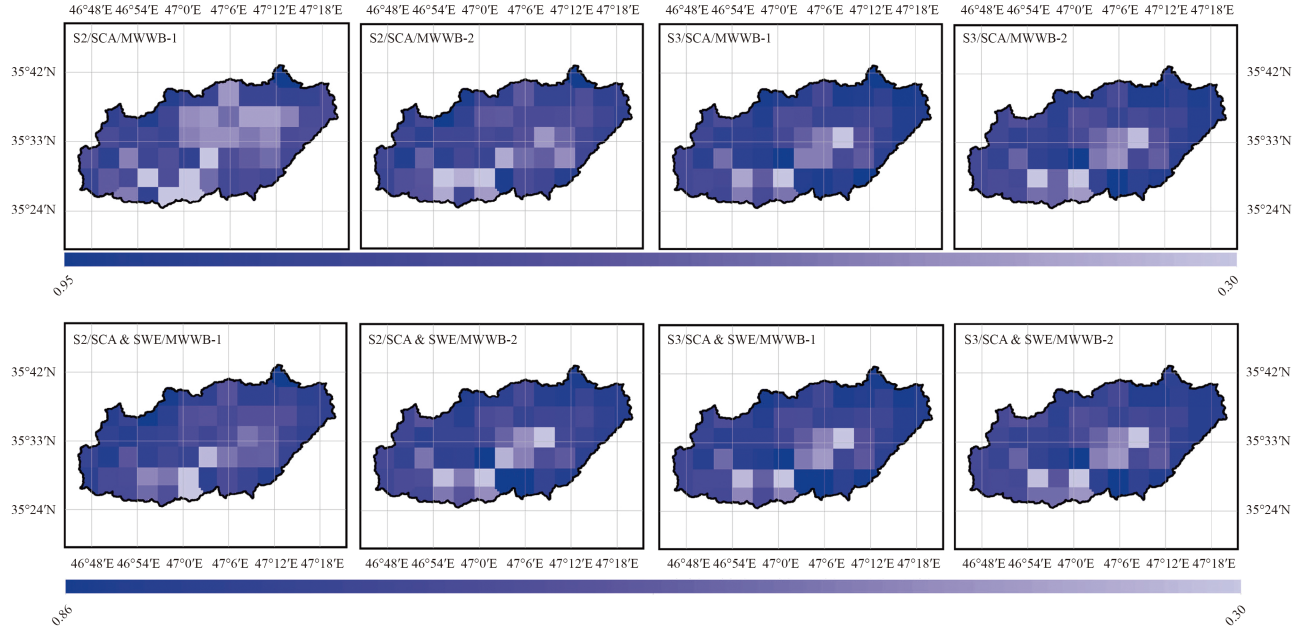


**Fig. 5** Spatial distribution of HSS for SCA variable in the second and third calibration scenarios using SCA and SWE&SCA.

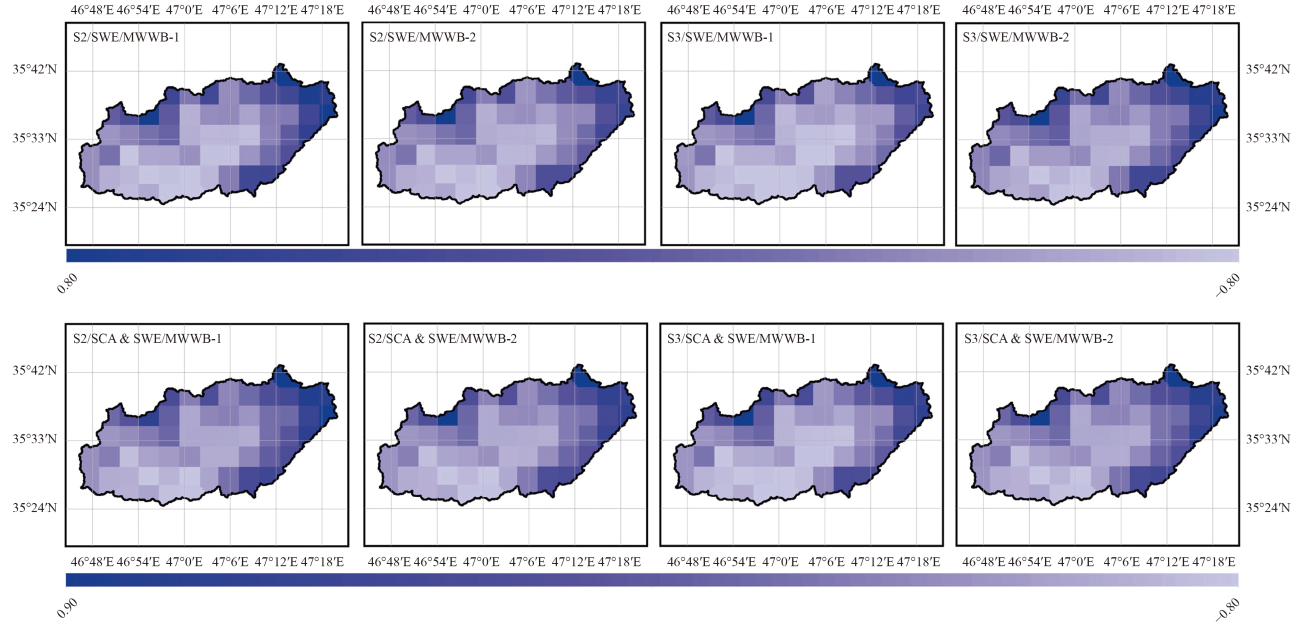


**Fig. 6** Spatial distribution of RE for SWE variable in the second and third calibration scenarios using SWE and SWE&SCA.

Table 3 lists the ratios of snowmelt to snowfall for different scenarios and models. Accordingly, the ratios varied between 0.83 and 0.98 for S2 and between 0.74 and 0.96 for S3. Given the fact that the ratios subtracted from one indicate the portion of the snowpack sublimation (ranging from 2% to 26%), the second scenario showed less snow sublimation than the third one. Moreover, the sublimation amount was insignificant for the MWWB-2 model, indicating the conversion of almost the entire snowfall to snowmelt. Similarly, the ratio of snowmelt to snowfall was calculated for each pair of data sets (i.e., SCA/SWE, SWE/SCA & SWE, and SCA/SCA & SWE). Accordingly, the SCA/SWE, SWE/SCA & SWE, and SCA/SCA & SWE varied between 0.95 and 1.03, 0.96–0.99, and 0.95–0.99, respectively, for S2 and between 0.95 and 1.04, 0.925–1.03, and 0.96–0.98, respectively for S3.

Given almost the same ratios (close to one), it was concluded that the conceptual structure of hydrological models and calibration processes had a suitable consistency and could provide an integrated response of the ratio of the snowmelt to snowfall using different scenarios and calibration references. It should be noted that the slight differences could be attributed to the

**Table 3** Contribution of snowmelt in generated streamflow and snowfall in the hydrologic models (the second and third calibration scenarios, and the three calibration references)

| | Scenario | SCA | SWE | SCA & SWE | SCA/SCA & SWE | SWE/SCA & SWE | SCA/SWE |
|---|---|---|---|---|---|---|---|
| **MWWB-1** | **Ratio of snowmelt to streamflow** | | | | | | |
| | **S2** | 0.763 | 0.728 | 0.807 | **0.945** | 0.902 | 1.048 |
| | **S3** | 0.612 | 0.591 | 0.627 | **0.977** | 0.942 | 1.037 |
| | **Ratio of snowmelt to snowfall** | | | | | | |
| | **S2** | 0.861 | 0.832 | 0.869 | 0.991 | 0.957 | 1.035 |
| | **S3** | 0.745 | 0.787 | 0.762 | 0.978 | 1.032 | 0.948 |
| **MWWB-2** | **Ratio of snowmelt to streamflow** | | | | | | |
| | **S2** | 0.759 | 0.746 | 0.725 | **1.047** | 1.030 | 1.017 |
| | **S3** | 0.713 | 0.682 | 0.710 | **1.004** | 0.961 | 1.045 |
| | **Ratio of snowmelt to snowfall** | | | | | | |
| | **S2** | 0.935 | 0.981 | 0.983 | 0.952 | 0.999 | 0.953 |
| | **S3** | 0.930 | 0.893 | 0.966 | 0.963 | 0.925 | 1.041 |

different structures in parametrizing the snowmelt and snowfall processes.

## 5 Conclusions and discussion

In the present research, GGSPs such as SCA and SWE were employed to calibrate hydrological models under three different scenarios to improve the accuracy of snowpack and streamflow simulations. The scenarios were defined based on one-stage (S1 and S3) and two-stage (S2) calibration approaches using SCA, SWE, and SCA & SWE products, as well as streamflow time series, as the calibration references. To implement the proposed scenarios in a mountainous watershed, a monthly water balance model (Wang et al., 2013) was modified using Guo and McCabe's snowpack modules, called MWWB-1 and MWWB-2, respectively.

The results revealed that multi-source calibration could improve modeling accuracy compared to situations in which the recorded streamflow was the only reference data used in the calibration procedure. Accordingly, the second and third scenarios outperformed the first scenario (benchmark), which was constructed only based on streamflow values in simulating the streamflow. The SWE product performed weaker than SCA in estimating the watershed streamflow, which could be due to the inherent uncertainty in the calculation process of the SWE product, spatial scale mismatch between the SWE data (10 km) and model (5 km), the smoothed orography caused by reanalysis resolution, and the assumption of constant snow density for the watershed (as a parameter obtained from the calibration). In addition, the individual use of snow products such as SCA and SWE as the calibration references provided more accurate results than the calibration using their combination. On the other hand, the two-stage calibration in which the snow module was calibrated independently from the main hydrological model not only increased the accuracy of the results (i.e., S2 outperformed S1 and S3, which were one-stage scenarios) but also decreased the number of calibration parameters, as well as the dependency of internal processes on the recorded streamflow.

According to the spatial patterns of SCA during the computational period, the most considerable difference between the observed and simulated SCA occurred in low-altitude areas of the watershed, likely due to the recurring fusion between cloud and snow caused by the monthly combination of daily snow errors. However, the high mountainous areas showed better performance in simulations using SCA. According to the spatial pattern of SWE, areas with very high and very low altitudes showed a misestimation of the simulated snow water equivalent compared to the reanalysis products since a constant snow density was assumed, while the highest compatibility of the simulated SWE with the products occurred in the middle altitudinal areas of the watershed.

The values of snowmelt contribution to the calculated generated streamflow for each pair of data sets (i.e., SCA/SWE, SWE/SCA & SWE, and SCA/SCA & SWE) varied within the ranges of 0.9–1.04 and 0.94–1.04 under scenarios S2 and S3, respectively. Since these values were almost the same (close to one), it could be concluded that the hydrological models had an appropriate consistency under different conditions (scenarios and calibration references), providing a reliable response to the meltwater contribution in the studied area. It should be noted that the slight differences could be attributed to the different structures in the parametrization of the snowmelt and snowfall processes.

Similarly, the ratios of snowmelt to snowfall, SCA/SWE, SWE/SCA & SWE, and SCA/SCA & SWE, varied between 0.95 and 1.03, 0.96–0.99, and 0.95–0.99, respectively, for S2. Meanwhile, these values ranged

between 0.95 and 1.04, 0.92–1.03, and 0.96–0.98, correspondingly, for S3. Given that all ratios were almost the same (close to one) for both S2 and S3, which used combinations of SCA, SWE, and SCA & SWE, they were reliable in providing an integrated response of the value of the snowmelt to snowfall for the studied area.

Further evaluations of hydrological models based on GGSPs using the received energy factor, along with the SCA and SWE products, are proposed for future studies. Considering the sensitivity assessment of the areas with the snow coverage ranging between 0% and 100% is another factor whose effect should be considered on the hydrological model independently.

## References


Ajami N K, Gupta H, Wagener T, Sorooshian S (2004). Calibration of a semi-distributed hydrologic model for streamflow estimation along with a river system. J Hydrol (Amst), 298(1−4): 112−135

Amini Y, Nasseri M (2021). Improving spatial estimation of hydrologic attributes via optimized moving search strategies. Arab J Geosci, 14(8): 723

Andreadis K M, Lettenmaier D P (2006). Assimilating remotely sensed snow observations into a macroscale hydrology model. Adv Water Resour, 29(6): 872–886

Beven K J (2011). Rainfall-Runoff Modeling: the Primer. New York: John Wiley & Sons

Bian Q, Xu Z, Zhao L, Zhang Y F, Zheng H, Shi C, Zhang S, Xie C, Yang Z L (2019). Evaluation and intercomparison of multiple snow water equivalent products over the Tibetan Plateau. J Hydrometeorol, 20(10): 2043–2055

Bigdeli M, Taheri M, Mohammadian A (2021). Spatial sensitivity analysis of COVID-19 infections concerning the satellite-based four air pollutants levels. Int J Environ Sci Technol, 18(3): 751–760

Chen X, Long D, Hong Y, Zeng C, Yan D (2017). Improved modeling of snow and glacier melting by a progressive two-stage calibration strategy with GRACE and multisource data: How snow and glacier meltwater contributes to the runoff of the Upper Brahmaputra River basin? Water Resour Res, 53(3): 2431–2466

Clark M P, Slater A G, Barrett A P, Hay L E, McCabe G J, Rajagopalan B, Leavesley G H (2006). Assimilation of snow-covered area information into hydrological and land-surface models. Adv Water Resour, 29(8): 1209–1221

Cline D, Elder K, Bales R (1998). Scale effects in a distributed snow water equivalence and snowmelt model for mountain basins. Hydrol Processes, 12(10−11): 1527−1536

Corbari C, Ravazzani G, Martinelli J, Mancini M (2009). Elevation-based correction of snow coverage retrieved from satellite images to improve model calibration. Hydrol Earth Syst Sci, 13(5): 639–649

Dai L, Che T, Ding Y (2015). Inter-calibrating SMMR, SSM/I and SSMI/S data to improve the consistency of snow-depth products in China. Remote Sens (Basel), 7(6): 7212–7230

Debele B, Srinivasan R, Gosain A K (2010). Comparison of process-based and temperature-index snowmelt modeling in SWAT. Water Resour Manage, 24(6): 1065–1088

Derksen C, Walker A, Goodison B (2005). Evaluation of passive microwave snow water equivalent retrievals across the boreal forest/tundra transition of western Canada. Remote Sens Environ, 96(3−4): 315−327

Dietz A J, Kuenzer C, Gessner U, Dech S (2012). Remote sensing of snow–a review of available methods. Int J Remote Sens, 33(13): 4094–4134

Dressler K A, Leavesley G H, Bales R C, Fassnacht S R (2006). Evaluation of gridded snow water equivalent and satellite snow cover products for mountain basins in a hydrological model. Hydrol Process, 20(4): 673–688

Duan Q, Sorooshian S, Gupta V (1992). Effective and efficient global optimization for conceptual rainfall-runoff models. Water Resour Res, 28(4): 1015–1031

Duethmann D, Peters J, Blume T, Vorogushyn S, Güntner A (2014). The value of satellite-derived snow cover images for calibrating a hydrological model in snow-dominated catchments in Central Asia. Water Resour Res, 50(3): 2002–2021

Engeset R V, Udnæs H C, Guneriussen T, Koren H, Malnes E, Solberg R, Alfnes E (2003). Improving runoff simulations using satellite-observed time-series of snow-covered areas. Nord Hydrol, 34(4): 281–294

Finger D, Pellicciotti F, Konz M, Rimkus S, Burlando P (2011). The value of glacier mass balance, satellite snow cover images, and hourly discharge for improving the performance of a physically based distributed hydrological model. Water Resour Res, 47(7)

Franz K J, Karsten L R (2013). Calibration of a distributed snow model using MODIS snow covered area data. J Hydrol (Amst), 494: 160–175

Gao H, Dong J, Chen X, Cai H, Liu Zh, Jin Zh, Mao D, Yang Z, Duan Z (2020). Stepwise modeling and the importance of internal variables validation to test model realism in a data scarce glacier basin. J Hydro, 591: 125457

Güntner A, Uhlenbrook S, Seibert J, Leibundgut C (1999). Multi-criterial validation of TOPMODEL in a mountainous catchment. Hydrol Processes, 13(11): 1603–1620

Guo S, Chen H, Zhang H, Xiong L, Liu P, Pang B, Wang G, Wang Y (2005). A semi-distributed monthly water balance model and its application in a climate change impact study in the middle and lower Yellow River basin. Water Int, 30(2): 250–260

Hall D K, Riggs G A (2007). Accuracy assessment of the MODIS snow products. Hydrol Processes, 21(12): 1534–1547

Hall D K, Riggs G A (2015). MODIS/Terra Snow Cover Monthly L3 Global 0.05Deg CMG, Version 6. Boulder, Colorado USA. NASA National Snow and Ice Data Center Distributed Active Archive Center

Hall D K, Riggs G A (2021). MODIS/Terra Snow Cover Monthly L3 Global 0.05Deg CMG, Version 61. Boulder, Colorado USA. NASA National Snow and Ice Data Center Distributed Active Archive Center

Han P, Long D, Han Z, Du M, Dai L, Hao X (2019). Improved understanding of snowmelt runoff from the headwaters of China's Yangtze River using remotely sensed snow products and hydrological modeling. Remote Sens Environ, 224: 44–59

He Z H, Parajka J, Tian F Q, Blöschl G (2014). Estimating degree day factors from MODIS for snowmelt runoff modeling. Hydrol Earth Syst Sci, 18(12): 4773–4789

Immerzeel W W, Droogers P, De Jong S M, Bierkens M F P (2009). Large-scale monitoring of snow cover and runoff simulation in Himalayan river basins using remote sensing. Remote Sens Environ, 113(1): 40–49

Jazim A A (2006). A monthly six-parameter water balance model and its application at arid and semiarid low yielding catchments. J King Saud U Eng Sci, 19(1): 65–81

Karpouzos D K, Baltas E A, Kavalieratou S, Babajimopoulos C (2011). A hydrological investigation using a lumped water balance model: the Aison River Basin case (Greece). Water Environ J, 25(3): 297–307

Khakbaz B, Imam B, Hsu K, Sorooshian S (2012). From lumped to distributed via semi-distributed: calibration strategies for semi-distributed hydrologic models. J Hydrol (Amst), 418−419: 61–77

Kim R S, Kumar S, Vuyovich C, Houser P, Lundquist J, Mudryk L, Durand M, Barros A, Kim E J, Forman B A, Gutmann E D, Wrzesien M L, Garnaud C, Sandells M, Marshall H P, Cristea N, Pflug J M, Johnston J, Cao Y, Mocko D, Wang S (2021). Snow Ensemble Uncertainty Project (SEUP): quantification of snow water equivalent uncertainty across North America via ensemble land surface modeling. Cryosphere, 15(2): 771–791

Knoben W J, Freer J E, Woods R A (2019). Inherent benchmark or not? Comparing Nash–Sutcliffe and Kling–Gupta efficiency scores. Hydrol Earth Syst Sci, 23(10): 4323–4331

Lévesque E, Anctil F, Van Griensven A N N, Beauchamp N (2008). Evaluation of streamflow simulation by SWAT model for two small watersheds under snowmelt and rainfall. Hydrol Sci J, 53(5): 961–976

Li X, Williams M W (2008). Snowmelt runoff modelling in an arid mountain watershed, Tarim Basin, China. Hydrol Processes, 22(19): 3931–3940

Li S, Liu M, Adam J C, Pi H, Su F, Li D, Liu Z, Yao Z (2021). Contribution of snow-melt water to the streamflow over the Three-River Headwater Region, China. Remote Sens (Basel), 13(8): 1585

Martinec J, Rango A, Roberts R (1994). The snowmelt runoff model user's manual. In: Baumgartner M F, ed. Geographica Bernensia. University of Berne

McCabe G J, Markstrom S L (2007). A monthly water-balance model driven by a graphical user interface (Vol. 1088). Reston, VA: US Geological Survey

Muñoz-Sabater J (2019). ERA5-Land monthly averaged data from 1981 to present. In: Copernicus Climate Change Service (C3S) Climate Data Store (CDS)

Nemri S, Kinnard Ch (2020). Comparing calibration strategies of a conceptual snow hydrology model and their impact on model performance and parameter identifiability. J Hydrol (Amst), 582: 124474

Orsolini Y, Wegmann M, Dutra E, Liu B, Balsamo G, Yang K, de Rosnay P, Zhu C, Wang W, Senan R, Arduini G (2019). Evaluation of snow depth and snow cover over the Tibetan Plateau in global reanalyses using *in situ* and satellite remote sensing observations. Cryosphere, 13(8): 2221–2239

Parajka J, Blöschl G (2008). The value of MODIS snow cover data in validating and calibrating conceptual hydrologic models. J Hydrol (Amst), 358(3−4): 240−258

Parajka J, Merz R, Blöschl G (2007). Uncertainty and multiple objective calibration in regional water balance modelling: case study in 320 Austrian catchments. Hydrol Processes, 21(4): 435–446

Pulliainen J (2006). Mapping of snow water equivalent and snow depth in boreal and sub-arctic zones by assimilating space-borne microwave radiometer data and ground-based observations. Remote Sens Environ, 101(2): 257–269

Rabuffetti D, Ravazzani G, Corbari C, Mancini M (2008). Verification of operational Quantitative Discharge Forecast (QDF) for a regional warning system? the AMPHORE case studies in the upper Po River. Nat Hazards Earth Syst Sci, 8(1): 161–173

Rao A R, Al-Wagdany A (1995). Effects of climatic change in Wabash river basin. J Irrig Drain Eng, 121(2): 207–215

Reed S, Koren V, Smith M, Zhang Z, Moreda F, Seo D J, Participants D M I P (2004). Overall distributed model intercomparison project results. J Hydrol (Amst), 298(1−4): 27−60

Refsgaard J C (1997). Parameterisation, calibration and validation of distributed hydrological models. J Hydrol (Amst), 198(1−4): 69−97

Riboust P, Thirel G, Le Moine N, Ribstein P (2019). Revisiting a simple degree-day model for integrating satellite data: implementation of SWE-SCA hystereses. J Hydrol Hydromech, 67(1): 70–81

Roebber P J (2009). Visualizing multiple measures of forecast quality. Weather Forecast, 24(2): 601–608

Rodell M, Houser P R (2004). Updating a land surface model with MODIS-derived snow cover. J Hydrometeorol, 5(6): 1064–1075

Roy A, Royer A, Turcotte R (2010). Improvement of springtime streamflow simulations in a boreal environment by incorporating snow-covered area derived from remote sensing data. J Hydrol (Amst), 390(1−2): 35−44

Seibert J (2000). Multi-criteria calibration of a conceptual runoff model using a genetic algorithm. Hydrol Earth Syst Sci, 4(2): 215–224

Shrestha M, Koike T, Hirabayashi Y, Xue Y, Wang L, Rasul G, Ahmad B (2015). Integrated simulation of snow and glacier melt in water and energy balance-based, distributed hydrological modeling framework at Hunza River Basin of Pakistan Karakoram region. J Geophys Res Atmos, 120(10): 4889–4919

Shrestha M, Wang L, Koike T, Tsutsui H, Xue Y, Hirabayashi Y (2014). Correcting basin-scale snowfall in a mountainous basin using a distributed snowmelt model and remote-sensing data. Hydrol Earth Syst Sci, 18(2): 747–761

Slater A G, Clark M P (2006). Snow data assimilation via an ensemble Kalman filter. J Hydrometeorol, 7(3): 478–493

Smith M B, Koren V, Zhang Z, Zhang Y, Reed S M, Cui Z, Moreda F, Cosgrove B A, Mizukami N, Anderson E A, Andreassian V, Lerat J, Loumagne C, Perrin C, Ribstein P, Gupta H V, Yilmaz K K, Pokhrel P, Wagener T, Butts M, Yamagata K, Sorooshian S, Khakbaz B, Behrangi A, Hsu K, Imam B, De Smedt F, Safari A, Tavakoli M, Li L, Wang X, Wu J, Yang C, Yang M, Yu Z, Gan T, Islam Z, Vieux B, Looper J, Xia Y, Mitchell K, Ek M, McIntyre N, Orellana B, Sivapalan M, Li H, Tian F, Ryu J, Arnold J, Whittaker G, Confesor R, Di Luzio M (2012). Results of the DMIP 2

Oklahoma experiments. J Hydrol (Amst), 418-419: 17–48

Şorman A A, Şensoy A, Tekeli A E, Şorman A Ü, Akyürek Z (2009). Modelling and forecasting snowmelt runoff process using the HBV model in the eastern part of Turkey. Hydrol Processes, 23(7): 1031–1040

Taheri M, Dolatabadi N, Nasseri M, Zahraie B, Amini Y, Schoups G (2020). Localized linear regression methods for estimating monthly precipitation grids using elevation, rain gauge, and TRMM data. Theor Appl Climatol, 142(1–2): 623–641

Taheri M, Mohammadian A, Ganji F, Bigdeli M, Nasseri M (2022). Energy-based approaches in estimating actual evapotranspiration focusing on land surface temperature: a review of methods, concepts, and challenges. Energies, 15(4): 1264

Tekeli A E, Akyürek Z, Şorman A A, Şensoy A, Şorman A Ü (2005). Using MODIS snow cover maps in modeling snowmelt runoff process in the eastern part of Turkey. Remote Sens Environ, 97(2): 216–230

Thirel G, Salamon P, Burek P, Kalas M (2013). Assimilation of MODIS snow cover area data in a distributed hydrological model using the particle filter. Remote Sens (Basel), 5(11): 5825–5850

Udnæs H C, Alfnes E, Andreassen L M (2007). Improving runoff modelling using satellite-derived snow covered area? Nord Hydrol, 38(1): 21–32

Vogel R M, Sankarasubramanian A (2003). Validation of a watershed model without calibration. Water Resour Res, 39(10)

Wang G Q, Zhang J Y, Xuan Y Q, Liu J F, Jin J L, Bao Z X, He R M, Liu C S, Liu Y L, Yan X L (2013). Simulating the impact of climate change on runoff in a typical river catchment of the Loess Plateau, China. J Hydrometeorol, 14(5): 1553–1561

Widén-Nilsson E, Halldin S, Xu C Y (2007). Global water-balance modelling with WASMOD-M: parameter estimation and regionalisation. J Hydrol (Amst), 340(1−2): 105−118.

Xu C Y (1999). Estimation of parameters of a conceptual water balance model for ungauged catchments. Water Resour Manage, 13(5): 353–368

Yang J W, Jiang L M, Lemmetyinen J, Luojus K, Takala M, Wu S L, Pan J M (2020). Validation of remotely sensed estimates of snow water equivalent using multiple reference datasets from the middle and high latitudes of China. J Hydrol (Amst), 590: 125499

Yatheendradas S, Lidard C D P, Koren V, Cosgrove B A, De Goncalves L G, Smith M, Geiger J, Cui Z, Borak J, Kumar S V, Toll D L, Riggs G, Mizukami N (2012). Distributed assimilation of satellite‐based snow extent for improving simulated streamflow in mountainous, dense forests: an example over the DMIP2 western basins. Water Resour Res, 48(9): 2011WR011347

Zaitchik B F, Rodell M (2009). Forward-looking assimilation of MODIS-derived snow-covered area into a land surface model. J Hydrometeorol, 10(1): 130–148

Zappa M, Pos F, Strasser U, Warmerdam P, Gurtz J (2003). Seasonal water balance of an Alpine catchment as evaluated by different methods for spatially distributed snowmelt modelling. Nord Hydrol, 34(3): 179–202